Spectroscopic speciation and Thermodynamic modeling to explain the degradation of *weathering steel* surfaces in SO_2 rich urban atmospheres

Julene Aramendia*, Leticia Gómez-Nubla, Kepa Castro and Juan Manuel Madariaga

Department of Analytical Chemistry, University of the Basque Country UPV/EHU, P.O.Box 644, E-48080 Bilbao, Spain *julene.aramendia@ehu.es

The characteristic protection ability of *weathering steel* can be affected by the environment in SO_2 rich urban atmospheres. Although sulphur dioxide can partially be oxidised to sulphur trioxide, both acid gases that can be dissolved either in the atmosphere or in the moisture film present on the steel surface, forming sulphurous and/or sulphuric acid, accelerating the corrosion of the material. Thermodynamic simulations, based on experimental data obtained by Raman and SEM-EDS techniques on different weathering steel sculptures located outside in Bilbao (Basque Country), were done to probe the role of SO_2 in the formation of several soluble sulphates, such as, rozenite ($FeSO_4 \cdot 4H_2O$) and retgersite ($NiSO_4 \cdot 6H_2O$). According to the results, it was also confirmed that the presence of atmospheric particles of calcium carbonate has not an outstanding negative role in the metal decaying process. However, the presence of high magnesium calcite (HMC) plays an important role in the formation of magnesioferrite, another decaying product present in the surface of the *weathering steel*. As all these sulphates are soluble, rain water can dissolve them leading into a continuous decaying and material loss process.

1. INTRODUCTION

The so called *weathering steel* (i.e. CorTen steel) is a special case regarding to corrosion. This material was developed to be used outdoors due to its low cost and high strength. [1] The corrosion rate of this material is considerably lower than that of the standard carbon steel. [2] This corrosion resistance is achieved by adding small amounts of certain elements to the steel such as nickel.[3]

In previous scientific studies, [4, 5] *weathering steel* sculptures, located outdoors in Bilbao city (Basque Country), with some conservation problems were analyzed. Those artworks revealed that analyzed *weathering steel* was undergoing a dissolving process of the surface. In fact, in the ground where the sculptures were located, a precipitate with high content of iron and nickel was found. [5] *Weathering steel* develops a characteristic protective rust layer that is formed mainly by lepidocrocite (γ-FeOOH), goethite (α-FeOOH), hematite (Fe_2O_3), magnetite

(Fe_3O_4) and akaganeite (β-FeOOH).[1, 4, 6-10] However, the only presence of these oxides cannot explain the observed dissolution process [4,5] because they have a very small solubility constant (Ks_0 around10^{-36}).

According to literature [11, 12], sulphur dioxide has been identified the main corrosive air pollutant affecting *weathering steel*. In high sulphur dioxide atmospheres (>22 μg/m^2 s) and at high relative humidity it is probed that sulphite and sulphide rich corrosion products can be formed, which are soluble, at least more soluble than iron oxides. This fact results into a material loss process. The dissolution process is favored because the high concentration of SO_2 reduces the pH and increases the corrosion rate of the metal.[13] In addition, in revised studies on *weathering steel*, [11, 12] soluble sulphates were identified in industrial atmospheres, such as rozenite ($FeSO_4$) and ferric sulphate ($Fe_2(SO_4)_3$), which are very soluble compounds, and are expected to be identified on the steel surfaces exposed to an industrial atmosphere.

The role of sulphates and their degradation pathways are well known in the decay of other kind of materials, such as wall paintings, pigments, stones and mortars[14-17]. In those cases, authors confirm, in fact, that SO_x is responsible of the formation of such sulphates. In *weathering steel*, however, the reactions that occur among the material and the different pollutants to give rise to the above mentioned iron sulphates are not very clear. Moreover, the degradation process of the dissolution of nickel in *weathering steels* is not reported in the revised literature.

Due to the lack of information, a study of the lixiviation process of the *weathering steel* due to high concentration of SO_2 in urban atmospheres is presented. Beside, the role of some atmospheric particles in the degradation of *weathering steel* was studied. The work is based on chemical equilibrium simulations by using thermodynamic software called *MEDUSA* (Make Equilibrium Diagrams Using Sophisticated Algorithms).[18] This software is based on SOLGASWATER and HALTAFALL algorithms.[19,20] *MEDUSA* allows to model chemical equilibriums in solution using the formation constants of the different compounds that are collected in an own database called HYDRA. The thermodynamic simulations were performed based on the results of Raman and SEM-EDS analysis of the analyzed *weathering steel* surfaces, following our strategy [14-16] to develop the required chemical models for such calculations [21, 22].

2. MATERIALS AND METHODS

The thermodynamic study was done after the analysis of several *weathering steel* (COR-TEN) sculptures made in the last decades of the 20th century. These COR-TEN steel sculptures are outdoors in Bilbao city (Basque Country, Northern Spain) and have been subjected to several environmental stressors, mainly to SO_x acid gases. In fact, the *weathering steel* structures showed an esthetically irregular surface due to the active process of corrosion.[5] Bilbao has a corrosion category C4, according to ISO 9223 [21], which is considered a high corrosion index. This fact is related to its high number of rainy days, to a high annual rainfall rate and to a high SO_2 pollution (81 mg/m^2 deposition rate). [12]

Spectroscopic data used for this study were acquired *in-situ* by Raman spectroscopy and only in some cases detached chips from the surface were analyzed in laboratory for a deeper study by SEM-EDS and by Raman imaging. The use of portable instrumentation was crucial in order to identify the degradation products in the state in which they are on the steel surface. This procedure is very important to assure the most accurate modeling of the chemical system.

For this purpose, Raman analyses were done by using a handheld InnoRam spectrometer (B&W Tek Inc., USA). The equipment is provided with a 785 nm excitation laser and a microprobe. In some cases and when the conditions were suitable, an X-Y-Z motorized automatic tripod (Microbeam, Spain) was employed. It was possible to focus the laser beam on a 10-200 µm spot, depending on the objective (10x, 20x, 50x). The equipment implements a software controller of the laser power (from 0 to 100%). In this way, the measures were performed at the maximum laser power that allowed achieving the best signal/noise ratio without thermodecomposition or mineral phase changes of the sample. Usually a 20% of the total laser power was enough to acquire a good signal without any mineral phase change. The calibration of the handheld instrument was performed everyday by using a silicon slice (Raman band at 520.5 cm^{-1}). The spectroscopic data were acquired with the BWSpec™ software version 3.26 (B&W Tek Inc., USA).

For spectral analysis and treatment, the Omnic software (Thermo Nicolet, USA) was used. The spectra interpretation was done by comparison with pure standard compounds contained in a homemade database [24] and with RRUFF online database [25].

In some cases, detached steel chips were sent to the laboratory in order to carry out a deeper study by Energy Dispersive Spectroscopy (EDS) mapping on Scanning Electron Microscopy (SEM). An EVO®40 Scanning Electron Microscope (Carl Zeiss NTS GmbH,

Germany) coupled to an X-Max Energy-Dispersive X-Ray spectroscopy equipment (Oxford Instruments, UK) was used for electron image acquisitions and elemental composition determinations of steel chips. The SEM images were acquired at high vacuum employing an acceleration voltage of 20 KV. It was reached up to 10000x using a secondary electron detector. The elemental mapping analysis (EDS) was performed using an 8.5 mm working distance, a 35º take-off angle and an acceleration voltage of 20KV.

For Raman imaging analyses a Renishaw InVia Raman micro spectrometer was used, coupled to a DMLM Leica microscope with 5x, 20x, 50x and 100x objectives. Images were acquired with the 514 nm laser, using the Stream Line device. The power applied was set at the source at a maximum of 50 mW while on the sample was always less than 20 mW.

The chemical and thermodynamic modeling of the steel dissolution process was carried out using Medusa software (*Make Equilibrium Diagrams Using Sophisticated Algorithms*).[18] The atmospheric chemical conditions used for the modeling were those measured *in-situ* or obtained from the officials air-quality monitoring stations. [26] Some physic-chemical parameters were measured on the dripping water coming from the sculptures when raining, using different Crison electrodes; Crison 52-02 electrode for pH measurements and Crison 52-61 for the redox potential.

3. RESULTS AND DISCUSSION

The main mineral phases present in the rust layer of these *weathering steel* sculptures were lepidocrocite, goethite, magnetite, akaganeite and hematite, together with other compounds identified on the surface of the steel samples present due to wet/dry deposition and to interaction between acid gases, the deposited atmospheric particles and the steel rust layer compounds, developing degradation compounds such as retgersite ($NiSO_4 \cdot 6H_2O$) and rozenite ($FeSO_4 \cdot 4H_2O$) that damage the steel surface. [4, 5, 11, 12]

Many of the mentioned particles could be seen microscopically (Figure S-1), and even macroscopically all over the surfaces. These particles were analyzed by means of different techniques. The element distribution maps, obtained by means of SEM-EDS (see Figure 1), detected the high deposition rates of calcium that are suffering the studied steel surfaces. Figure 1 shows particles of calcium and some particles of magnesium together with particles where calcium and magnesium were present. In the false color image calcium's energies are

represented in green, magnesium's and silicon's energies in orange and the background, mainly iron, in blue.

Raman spectroscopy shown that calcium and magnesium were linked to the presence of different carbonates deposited on lepidocrocite (Raman main band at 250 cm^{-1}) [4]. Lepidocrocite was the main iron phase found in the rust layer. Raman imaging done over *weathering steel* surfaces (Figure 2) showed the presence of many calcite particles ($CaCO_3$, main Raman band at 1085 cm^{-1}) and high magnesium calcite particles (HMC, main band at 1090 cm^{-1}). [5, 27] HMC is a very common particulate material in the atmospheres of the cities in the Basque Country [28].

The presence of carbonates and other basic particulate matter, like aluminate compounds, seems to favored the SO_x gas and ammonium sulphate (typical compound in the atmosphere of Bilbao) interactions with the surface of the steel, transforming and developing new degradation products such as calcium and magnesium sulphate, felsobanyaite ($Al_4(SO_4)(OH)_{10}\cdot 5H_2O$) and so on. It is widely known that the SO_x can produce corrosion problems in many different materials, [29, 30] actually, by means of *in-situ* Raman spectroscopy, retgersite ($NiSO_4\cdot 6H_2O$, main Raman band at 987 cm^{-1}, Figure 3) and rozenite ($FeSO_4\cdot 4H_2O$, main Raman band at 991 cm^{-1}, Figure 3) were even detected. It is worth pointing out that the number of times in which retgersite was detected was significantly higher comparing to the case of rozenite. Therefore, it can be said that the presence of nickel sulphate is higher than the presence of rozenite. In addition, in previous works it was seen that the amount of dissolved nickel in the *weathering steel* surfaces was higher than the amount of iron.[5]

Taking into account the spectroscopic results, a hypothesis for the formation of these sulphates was proposed: The SO_x gases present in Bilbao atmosphere attack the steel through the calcite and the HMC, producing gypsum ($CaSO_4\cdot 2H_2O$) and enough concentration of dissolved sulphate to form rozenite and retgersite. This hypothesis is based on the degradation pathways described for other materials [14-17]. Then, rain wash can dissolve rozenite, retgersite and the other formed soluble sulphates given rise to a loss of material and to the conservation and aesthetic problems found on the surface of the steel.

In order to probe the hypothesis of how rozenite and retgersite can be formed, thermodynamic chemical simulation was done using the *MEDUSA* software. For this purpose, it was crucial to define perfectly the different chemical conditions in which the equilibrium reaction was developing. Dripping water coming from the different sculptures was collected and measured *in-situ* in order to establish the pH and the redox potential. Redox potential varied from 89 to 91 mV, thus, it was decided to set it at 90 mV. The measured pH values varied from 5 to 8 (usually less than 7). This variation can be explained due to the heterogeneity of the steel surface conditioned by the micro pores and cracks where the water and basic calcareous particles are accumulated. Thus, the conditions can vary quite a lot, giving raise to different micro chemical conditions depending on the particles or gases that are dissolved in each pore. Therefore, it was decided to set the pH at 5-6 as an agreement, but always taking into account the possibility of heterogeneity. The temperature used for the simulations was 25ºC in all cases.

The main and the most relevant pollutant gases present in the environment of Bilbao are SO_2 and CO_2. Thus, they were used as atmospheric stressors in the chemical simulation. Their atmospheric concentrations were obtained from the air quality vigilance network of the Basque Country Government. [26] In order to specify the concentration of steel components such as iron and nickel, data from the steelwork information was collected.

The legends present in the diagrams obtained with the *MEDUSA* software (Figures 4, 5, 6) show the molar concentrations values of the initial components. The concentration of SO_2 is represented in the *X* axis, increasing from 0 to 400 mM, in order to assess the pernicious effect of SO_2 gas simulating an accumulative effect. The effect of CO_2 was also considered and introduced in the inputs as H_2CO_3. Different chemical forms of Fe and Ni were tested as starting chemical phases in the inputs for the simulation of the chemical system. On the one hand, Fe(0) and Ni(0) were tested and on the other hand their respective most stable oxides. In the case of iron oxide, *MEDUSA* represents them as $Fe(OH)_3$ and in the case of nickel, as NiO. However, as it can be seen in Figure 4 and 5, the obtained results were independent from the chemical forms of Fe and Ni in the input. In fact, redox and pH equilibrium conditions determined that the initial phase of Fe is magnetite (Fe_3O_4). Magnetite was identified by *in-situ* Raman spectroscopy and it is produced due to a partial reduction of iron (III) oxides, present in the surfaces of the *weathering steel*, induced by atmospheric SO_2.

In order to ascertain the role of the atmospheric particles deposited on the steel surface, two chemical systems were considered, with and without calcite. In fact, the thermodynamic study tried to simulate the reactions taking place in the surroundings of the calcareous particles (Figure S-1 left). As expected, the thermodynamic simulation showed that calcite is attacked by

SO_2 giving rise to different hydration forms of calcium sulphate (Figure S-2). The presence of different hydration forms of calcium sulphate all over the surface of the steel structures was corroborated by the *in-situ* Raman analyses.[5] However, the diagrams present in Figures 4a-d show that the presence of calcite in the steel surface is not decisive for the formation of rozenite. This fact means that the SO_2 concentration present in the atmosphere of Bilbao is enough to react directly with iron from the steel generating rozenite. Thus, the partial dissolution of gypsum is not needed for the formation of rozenite, which contradicts the initial hypothesis.

The formation of rozenite is pH dependent. For example, at 200 mM of SO_2, the molar fraction of rozenite is 0.134 at pH 6.0 (Figure 4c, 4d), whereas it is 0.186 at pH 5.8 (Figure 4e, 4f). Thus, the accumulation and the rise of concentration of acid gases such as CO_2, NO_x and SO_x decrease the pH of the rain water, increasing the damage of the steel structures. Hence, this effect of pH in the degradation of *weathering steel*, i.e., in the formation of rozenite, is very relevant in the Bilbao environment where the measured pH value of the rainwater is around 5,0-5,5. Figure 4also shows how the presence of calcium carbonate requires a higher concentration of SO_2 to form rozenite, because calcite must be neutralized first by SO_2, developing $CaSO_4$,[5] and then magnetite can react with SO_2 to form rozenite. The formation of gypsum is also predicted (Figure S-2).

Rozenite could be formed either as a direct attack to magnetite (reaction 1) done by H_2SO_4 aerosol (oxidation of SO_2 in high humid atmosphere) or as a direct attack to any other iron (III) oxide phase (reaction 2) after a partial reduction by SO_2 in presence of protons (i.e. H_2CO_3 or even HNO_3 from oxidized NO_x).

$$Fe_3O_4 + H_2SO_4 + 4H_2O \rightarrow FeSO_4{\cdot}4H_2O + Fe_2O_3 + H_2O \qquad \text{(reaction 1)}$$

$$Fe_2O_3 + SO_2 + 2H^+ + 3H_2O \rightarrow FeSO_4{\cdot}4H_2O + Fe^{2+} \qquad \text{(reaction 2)}$$

The presence of hematite (Fe_2O_3) in the steel surface, as the starting compound to form rozenite (reaction 2), is supported by some experimental evidences published by *de la Fuente et al*. [12] In that work, several steel samples exposed to different environments were studied, and Bilbao was selected as an example of industrial atmosphere. They mention that hematite was only identified on steel samples exposed in Bilbao and no hematite was identified in the other atmospheres. Additionally, they affirm that hematite is not commonly cited in the literature consulted. In contrast, in the sculptures considered in the present study hematite was very commonly detected in all cases. [4]

In the case of retgersite ($NiSO_4 \cdot 6H_2O$), the formation pathway is the same as for the rozenite. As the formation stability constant of retgersite is higher than that of rozenite, the molar fraction of retgersite is higher than that of rozenite at the same experimental conditions. This fact was checked also by Raman spectroscopy (Figure 3), as the relative presence of retgersite was higher than the relative presence of rozenite in all the collected spectra. Relative presence means an estimation based on the number of times that a mineral compound appeared in the whole set of spectra acquired for each sculpture, that was always more than 100 measurements per sculpture. There is another difference with regard to the degradation of iron species. In the case of Ni, at low concentrations of SO_2 gas, and in presence of carbonates, a nickel carbonate is formed. However, this mineral phase could not be detected by Raman spectroscopy. This fact could mean that, in general, the range of concentration of SO_2 in which nickel carbonate is formed is always exceeded in Bilbao atmosphere or that the concentration of nickel carbonate is very low, and thus, nor detectable by Raman spectroscopy. The differences in the diagrams (not shown) due to the pH fluctuation are not as remarkable as in the case of rozenite. In addition, as in the case of rozenite, calcite competes with nickel for the SO_2 and the fraction of formed retgersite depends on the presence or the absence of calcite (Figure 5).

Keeping in mind that redox conditions of Bilbao are enough to oxide Ni^0 to NiO, retgersite could be formed either as a direct attack to NiO (reaction 3) done by H_2SO_4 aerosol or as a direct attack to nickel carbonate (reaction 4).

$$NiO + H_2SO_4 + 5H_2O \rightarrow NiSO_4 \cdot 6H_2O \qquad \text{(reaction 3)}$$

$$NiCO_3 + H_2SO_4 + 5H_2O \rightarrow NiSO_4 \cdot 6H_2O + CO_2 \qquad \text{(reaction 4)}$$

Further thermodynamic simulations were done taking into account the presence of HMC particles. As in the case of calcite, several pH values were taken into account. At pH values measured in dripping rain water from sculptures (from 5 to 8) the thermodynamic simulations confirm the formation of epsomite ($MgSO_4 \cdot 7H_2O$), experimentally identified by Raman spectroscopy. [5] However, at pH values higher than 8 (Figure 6), *MEDUSA* shows the formation of magnesioferrite ($MgFe_2O_4$), also detected by Raman spectroscopy on the *weathering steel* surfaces (Figure 3). Thus, Raman evidences seem to support the conclusion of the thermodynamic study. Magnesioferrite exists at low concentration of SO_2, from 0 to 150 mM, and its molar fraction decreases as the concentration of SO_2 increases. This means that the existence of magnesioferrite depends strongly on the pH, and needs basic pH values. These values can only be reached in the surroundings of HMC particles, being a reaction that occurs in the interface of the particle and the steel surface.

Finally, the presence of fesolbanyaite ($Al_4(SO_4)(OH)_{10}\cdot 5(H_2O)$) was also detected in the steel surface. The formation of this compound was simulated by *Medusa* in the studied conditions. The simulation confirmed that this sulphate was formed from an aluminosilicate, as it was proposed in previous works.[5]

4. CONCLUSIONS

The compounds identified by the spectroscopic data analysis (rozenite and retgersite) in the surface of *weathering steel* sculptures, have been confirmed by the thermodynamic modeling. These mineral phases are produced by chemical reactions among the original components of the steel, iron and nickel in this case, and the acid gases (SO_2) present in the atmosphere.

The high formation constant of the retgersite makes the nickel sulphate fraction higher than the rozenite fraction, even though nickel is 100 times less concentrated in the alloy formulation. This fact, support the high relative presence of retgersite detected by Raman spectroscopy and the high amount of dissolved nickel measured in previous works [5]. Although nickel is added to *weathering steel* alloys to increase the resistance of the material against the corrosion, as metallic nickel is highly dissolved due to the SO_2 presence, the protective function of nickel in the *weathering steel* seems to be seriously decreased in SO_2 rich urban atmospheres.

In addition, iron is also dissolved due to the reaction with sulfur dioxide, and with this study it has been demonstrate that the presence of SO_2 in the atmosphere can produce material loss in *weathering steel*.

MEDUSA also has predicted the formation of other compounds due to the interaction of steel surface and atmospheric particles (HMC, calcium carbonate, silicates), such as epsomite, magnesioferrite and fesolbanyaite. However, atmospheric particles do not carry out a key role in the lixiviation process of the surface. Moreover, the presence or the absence of these particles do not affect to the formation of rozenite or retgersite, and the dissolution of the surface through the formation of those soluble iron and nickel sulphates can take place with or without the presence of such particles.

The presence of pores, cracks and irregularities on the surface of the steel can lead to the formation of micro-chemical systems with very different characteristics (pH, redox, etc) if basic particles and water remain retained inside those irregularities, giving rise to very specific decaying compounds such as magnesioferrite.

ACKNOWLEDGEMENTS

J. Aramendia and L. Gomez-Nubla are grateful to the Basque Government and to the University of the Basque Country (UPV-EHU) for their pre-doc fellowships. We would like to thank Bilbao Guggenheim Museum, BBVA bank and Bilbao City Council for all the support during the analysis of the sculptures. This work has been financially supported by DEMBUMIES project (ref. BIA2011-28148), funded by Spanish Ministry of Economy and Competitiveness. Authors thank Raman-LASPEA Laboratory from the SGIker (UPV/EHU, MICINN, GV/EJ, ERDF and ESF) of the University of the Basque Country for their collaboration in the analyses.

REFERENCES

(1) Decker, P.; Brüggerhoff, S.; Eggert, G. *Mater. Corros.* **2008**, *59*, 239-247.

(2) Choi, Y. S.; Kim, J. G. *Mater. Sci. Technol.* **2003**,*19*, 1737-1745.

(3) Damgaard, N.; Walbridge, S.; Hansson, C.; Yeung, J. *J. Constr. Steel Res.* **2010**, *66*, 1174-1185.

(4) Aramendia, J.; Gomez-Nubla, L.; Castro, K.; Martinez-Arkarazo, I.; Vega, D.; Sanz López de Heredia, A.; García Ibáñez de Opakua, A.; Madariaga, J. M. *J. Raman Spectrosc.* **2012**, *43*, 1111-1117.

(5) Aramendia, J.; Gomez-Nubla, L.; Arrizabalaga, I.; Prieto-Taboada, N.; Castro, K.; Madariaga, J.M. *Corros. Sci.* **2013** DOI: 10.1016/j.corsci.2013.06.038.

(6) Waseda, Y.; Suzuki, S. *Characterization of Corrosion Products on Steel Surfaces*, Springer; Sendai, 2005.

(7) Kimura, M.; Kihira, H. *Nippon Steel Tech. Rep.* **2005**, *91*, 86-90.

(8) Antunes, R.A.; Costa, I.; Araujo de Faria, D.L. *Mater. Res.* **2003**, *3*, 403-408.

(9) Kamimura, T.; Hara, S.; Miyuki, H.; Yamashita, M.; Uchida, H. *Corros. Sci.* **2006**, *48*, 2799-2812.

(10) Mi, F.; Wang, X.; Liu, Z.; Wang, B.; Peng, Y.; Tao, D. *J. Iron Steel Res.* **2011**, *18*, 67-73.

(11) Oesch, S. *Corros. Sci.* **1996**, *38*, 1357-1368.

(12) de la Fuente, D.; Díaz, I.; Simancas, J.; Chico, B.; Morcillo, M. *Corros. Sci.* **2011**, *53*, 604-617.

(13) Wang, J.H.; Wei, F.I.; Chang, Y.S.; Shih, H.C. *Mater. Chem. Phys.* **1997**, *47*, 1-8.

(14) Castro, K.; Sarmiento, A.; Martinez-Arkarazo, I.; Madariaga, J.M.; Fernández, L.A. *Anal. Chem.* **2008**, *80*, 4103-4110.

(15) Maguregui, M.; Knuutinen, U.; Martinez-Arakarazo, I.; Castro, K.; Madariaga, J.M. *Anal. Chem.* **2011**, *83*, 3319-3326.

(16) Maguregui, M.; Knuutinen, U.; Castro, K.; Madariaga, J.M. *J. Raman Spectrosc.* **2010**, *41*, 1110-1119.

(17) Sarmiento, A.; Maguregui, M.; Martinez-Arkarazo, I.; Angulo, M.; Castro, K.; Olazábal, M. A.; Fernández, L. A.; Rodríguez-Laso, M. D.; Mujika, A. M.; Gómez, J.; Madariaga, J. M. *J. Raman Spectrosc.* **2008**, *39*, 1042-1049.

(18) Puigdomenech, I. *MEDUSA (Make Diagrams Using Sophisticated Algorithms)*, version 15; Department of Inorganic Chemistry, The Royal Institute of Technology: Stockholm, Sweden. http://www.kth.se/che/medusa (last accessed July 2013)

(19) Eriksson, G. *Anal. Chim. Acta*. **1979**, *112*, 375-383.

(20) Ingri, N.; Kakolowicz, W.; Sillén, L.G.; Warnqvist, B. *Talanta*. **1967**, *14*, 1261-1286. Errata: 15(3) (1968) xi-xii.

(21) Raposo, J.C.; Sanz, J.; Borge, G.; Olazabal, M.A.; Madariaga, J.M. *Fluid Phase Equil.*, **1999**, *155*, 1-19.

(22) Belaustegi, Y.; Olazabal, M.A.; Madariaga, J.M. *Fluid Phase Equil.*, **1999**, *155*, 21-31

(23) ISO 9223, Corrosion of Metals and Alloys – Classification of Corrosivity of Atmospheres, ISO, Geneva, **1990**.

(24) Castro, K.; Pérez-Alonso, M.; Rodríguez-Laso, M. D.; Fernández, L. A.; Madariaga, J. M. *Anal. Bioanal. Chem.* **2005**, *382*, 248-258.

(25) R. T. Downs, Program and Abstracts of the 19th General Meeting of the International Mineralogical Association in Kobe, Japan. **2006**; O03, 13; http://rruff.info

(26) Homepage of Instituto Geográfico Nacional, Spain, http://www.ign.es/espmap/mapas_clima_bach/Mapa_clima_07.htm, (last accessed April 2013).

(27) Bischoff, W. D.; Sharma, S. K.; MacKenzie, F. T. *Am. Mineral.* **1985**, *70*, 581-589.

(28) Inza, A. Estudio de series temporales y de composición química del material particulado atmosférico en distintas áreas del País Vasco. Ph.D. Thesis UPV-EHU, Leioa, 2010.

(29) Kladkaew, N.; Idem, R.; Tontiwachwuthikul P.; Saiwan C. *Ind. Eng. Chem. Res*. **2009**, *48*, 10169–10179.

(30) Castaño, J.G.; Arroyave, C.; Morcillo, M. *J. Mater. Sci.* **2007**, *42*, 9654–9662.

FIGURE CAPTIONS

Figure 1. a) SEM image of a *weathering steel* sample. b) False color image done over the SEM image where calcium is represented in green color, magnesium and silicon in orange and iron in blue. In the middle, EDS maps for iron, calcium and magnesium are represented. On the bottom, EDS spectra of the most abundant particles present on the surface are shown.

Figure 2.Raman image of *weathering steel* surface (on the right). Lepidocrotite is represented in green color and the calcite particles in violet color.

Figure 3. Raman spectra of a) akaganeite (A), hematite (H) and rozenite(R) and b) lepidocrocite (L) and magnesioferrite (M) spectrum and c) retgersite (Re).

Figure 4. *MEDUSA* diagrams of rozenite formation on weathering steel surfaces.

Figure 5. Chemical simulation by *MEDUSA* software of the retgersite formation over *weathering steel* surfaces: in presence of calcite (a, c) and in absence of calcite (b, d).

Figure 6. *MEDUSA* diagrams showing the formation of epsomite and magnesioferrite over *weathering steel* surfaces.

Figure S-1. On the right, a microscopically picture of a calcite deposition. On the left, a graphical representation of the same picture where the calcite is represented in red, and in yellow the area where the spectroscopic and thermodynamic study was conducted. The background (iron oxides) is represented in blue.

Figure S-2. *MEDUSA* diagram of gypsum formation from a calcite particle over *weathering steel* surfaces exposed to an urban atmosphere, like that of Bilbao.

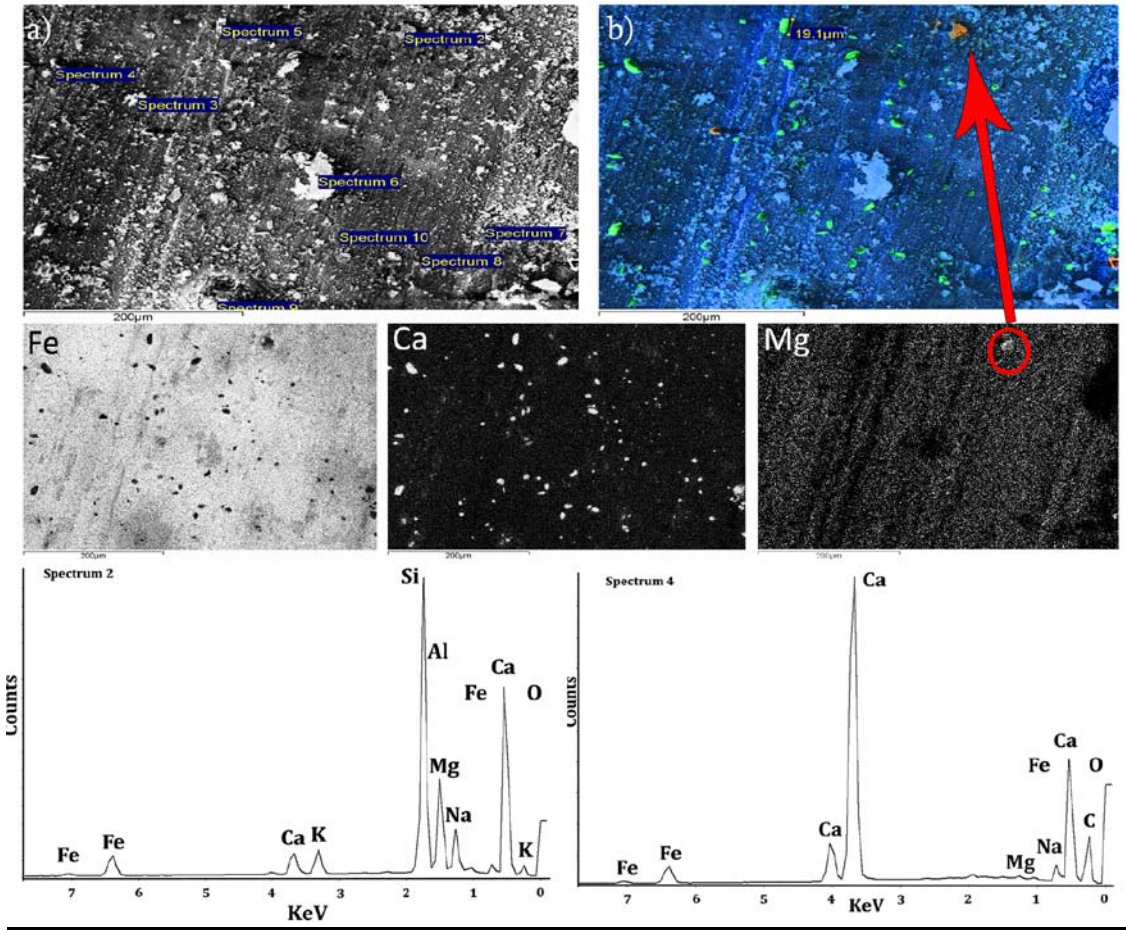

Figure 1

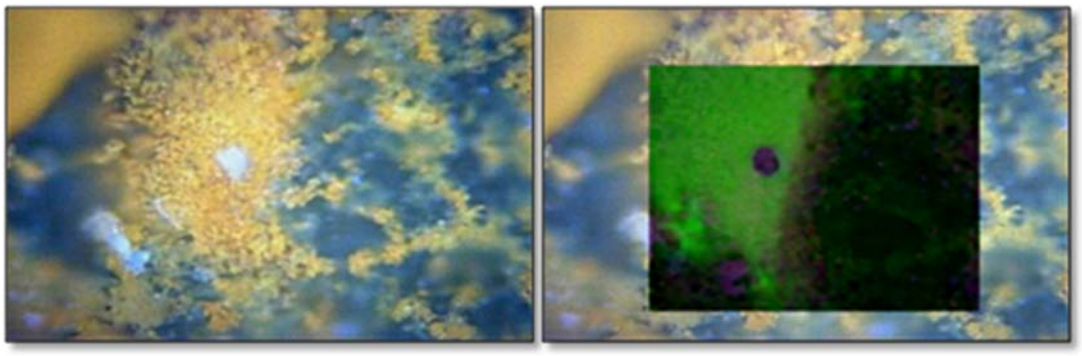

Figure 2

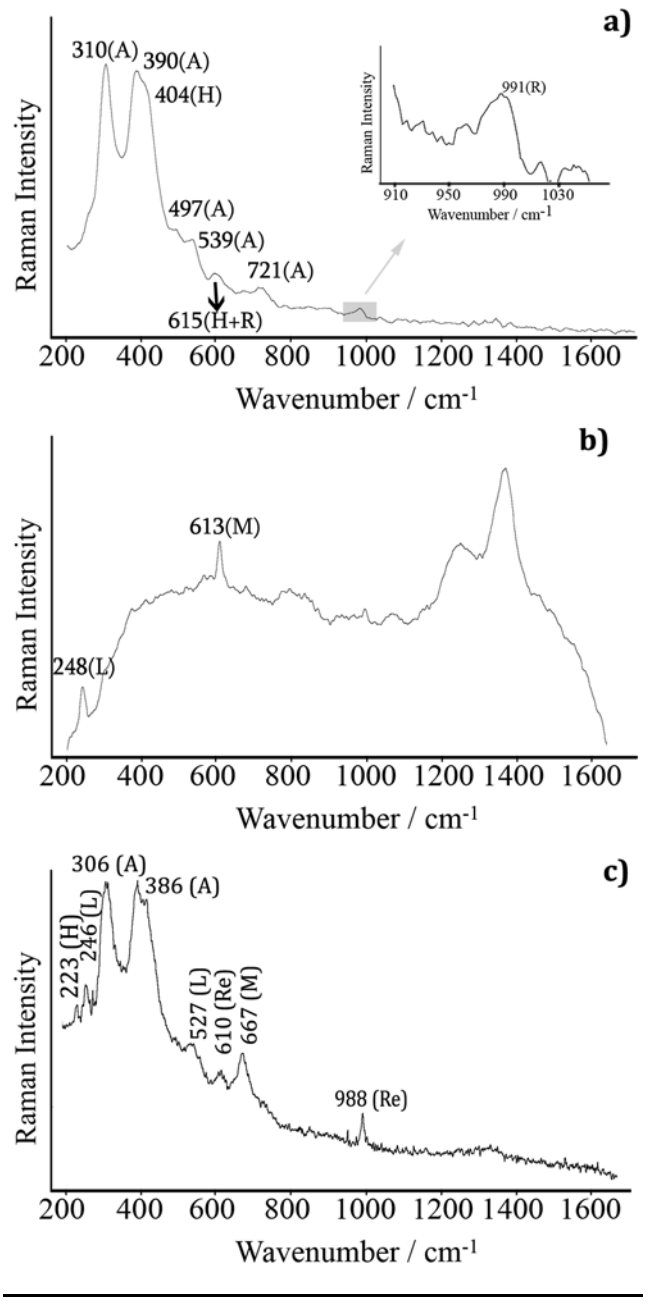
a)
310(A)
390(A)
404(H)
497(A)
539(A)
721(A)
615(H+R)
991(R)
Raman Intensity
910 950 990 1030
Wavenumber / cm-1
200 400 600 800 1000 1200 1400 1600
Wavenumber / cm-1
b)
613(M)
248(L)
Raman Intensity
200 400 600 800 1000 1200 1400 1600
Wavenumber / cm-1
c)
306 (A)
386 (A)
223 (H)
246 (L)
527 (L)
610 (Re)
667 (M)
988 (Re)
Raman Intensity
200 400 600 800 1000 1200 1400 1600
Wavenumber / cm-1

Figure 3

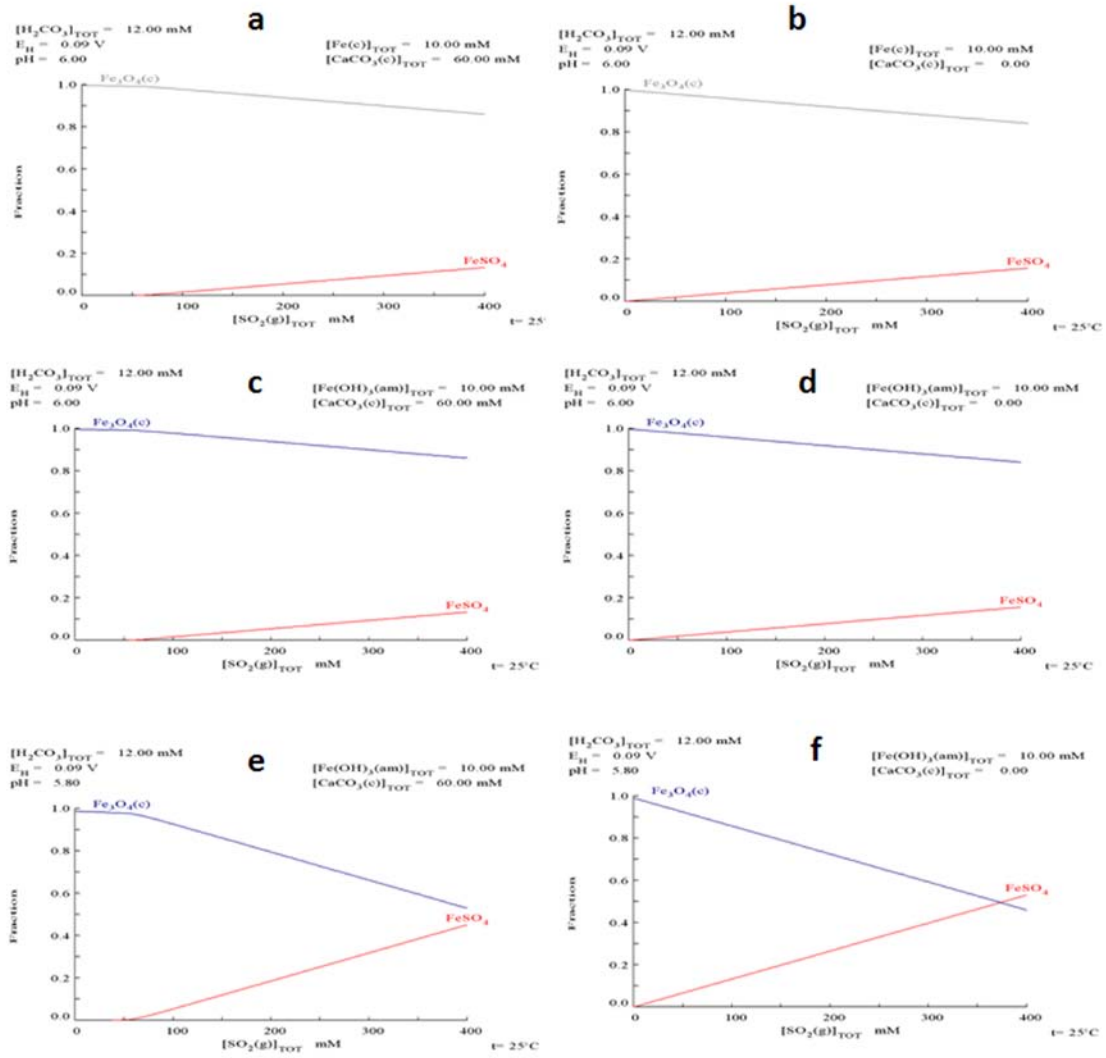
a
[H2CO3]TOT = 12.00 mM
EH = 0.09 V
pH = 6.00
[Fe(c)]TOT = 10.00 mM
[CaCO3(c)]TOT = 60.00 mM
Fe3O4(c)
FeSO4
Fraction
[SO2(g)]TOT mM
b
[H2CO3]TOT = 12.00 mM
EH = 0.09 V
pH = 6.00
[Fe(c)]TOT = 10.00 mM
[CaCO3(c)]TOT = 0.00
Fe3O4(c)
FeSO4
Fraction
[SO2(g)]TOT mM
t= 25°C
c
[H2CO3]TOT = 12.00 mM
EH = 0.09 V
pH = 6.00
[Fe(OH)3(am)]TOT = 10.00 mM
[CaCO3(c)]TOT = 60.00 mM
Fe3O4(c)
FeSO4
Fraction
[SO2(g)]TOT mM
t= 25°C
d
[H2CO3]TOT = 12.00 mM
EH = 0.09 V
pH = 6.00
[Fe(OH)3(am)]TOT = 10.00 mM
[CaCO3(c)]TOT = 0.00
Fe3O4(c)
FeSO4
Fraction
[SO2(g)]TOT mM
t= 25°C
e
[H2CO3]TOT = 12.00 mM
EH = 0.09 V
pH = 5.80
[Fe(OH)3(am)]TOT = 10.00 mM
[CaCO3(c)]TOT = 60.00 mM
Fe3O4(c)
FeSO4
Fraction
[SO2(g)]TOT mM
t= 25°C
f
[H2CO3]TOT = 12.00 mM
EH = 0.09 V
pH = 5.80
[Fe(OH)3(am)]TOT = 10.00 mM
[CaCO3(c)]TOT = 0.00
Fe3O4(c)
FeSO4
Fraction
[SO2(g)]TOT mM
t= 25°C

Figure 4

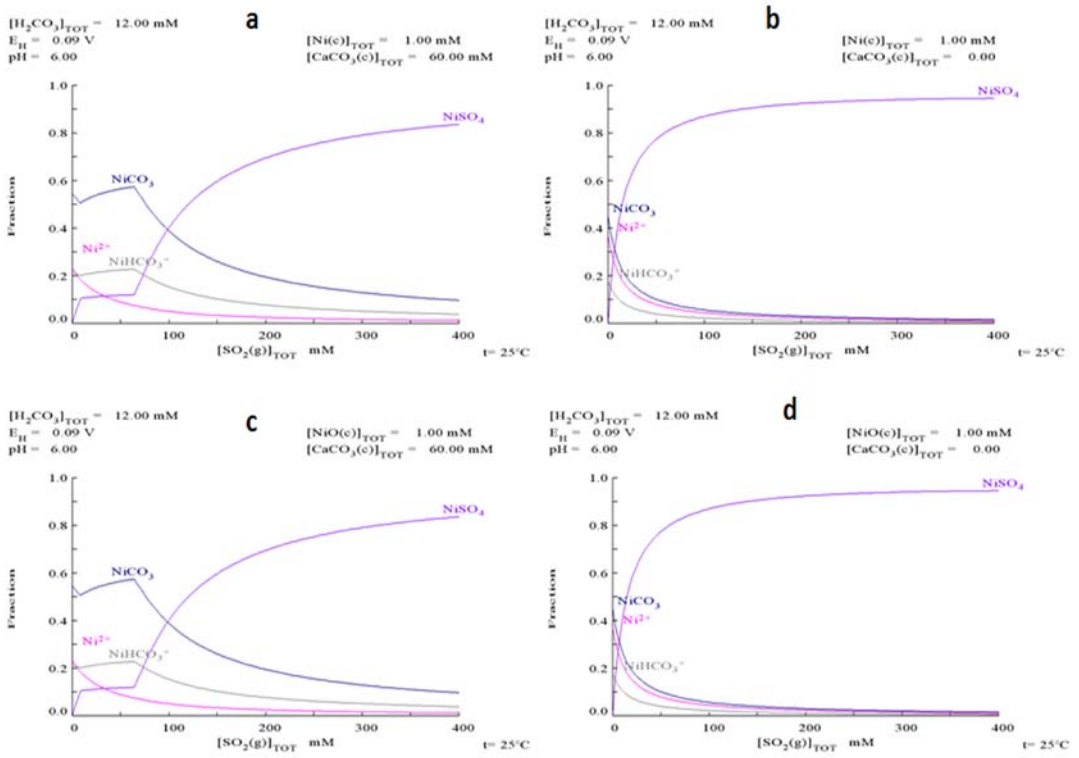
a
$[H_2CO_3]_{TOT}$ = 12.00 mM
E_H = 0.09 V
pH = 6.00
$[Ni(c)]_{TOT}$ = 1.00 mM
$[CaCO_3(c)]_{TOT}$ = 60.00 mM
b
$[H_2CO_3]_{TOT}$ = 12.00 mM
E_H = 0.09 V
pH = 6.00
$[Ni(c)]_{TOT}$ = 1.00 mM
$[CaCO_3(c)]_{TOT}$ = 0.00
c
$[H_2CO_3]_{TOT}$ = 12.00 mM
E_H = 0.09 V
pH = 6.00
$[NiO(c)]_{TOT}$ = 1.00 mM
$[CaCO_3(c)]_{TOT}$ = 60.00 mM
d
$[H_2CO_3]_{TOT}$ = 12.00 mM
E_H = 0.09 V
pH = 6.00
$[NiO(c)]_{TOT}$ = 1.00 mM
$[CaCO_3(c)]_{TOT}$ = 0.00
Fraction
$[SO_2(g)]_{TOT}$ mM
t= 25°C
$NiSO_4$
$NiCO_3$
Ni^{2+}
$NiHCO_3^+$

Figure 5

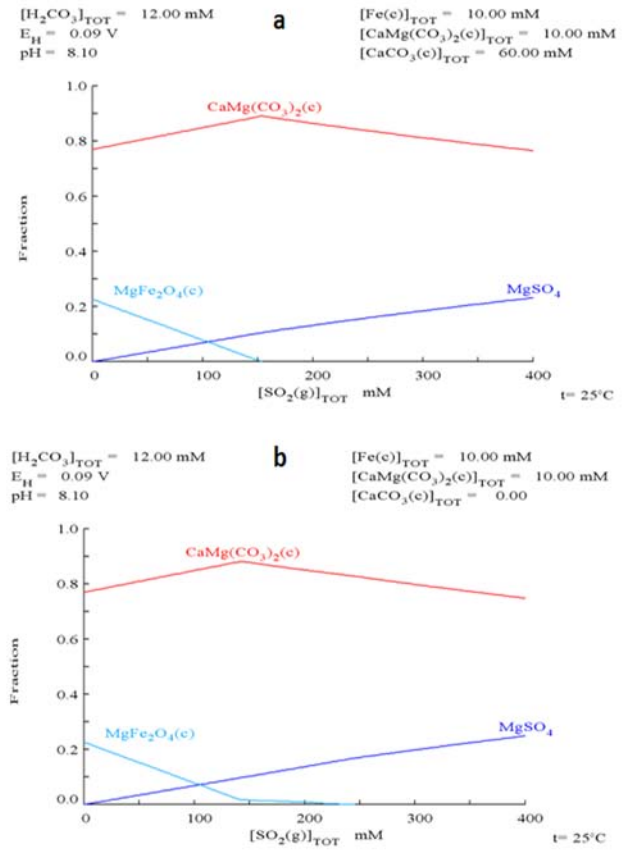

Figure 6

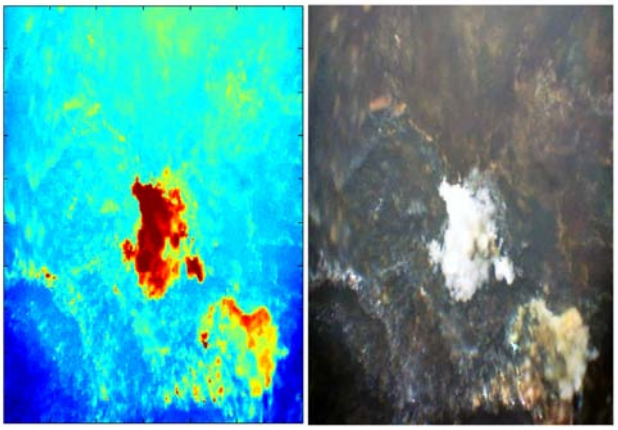

Figure s1

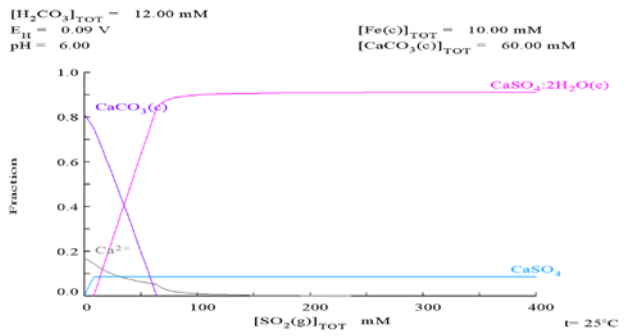
[H2CO3]TOT = 12.00 mM
EH = 0.09 V
pH = 6.00
[Fe(c)]TOT = 10.00 mM
[CaCO3(c)]TOT = 60.00 mM
CaSO4:2H2O(c)
CaCO3(c)
Ca2+
CaSO4
Fraction
1.0
0.8
0.6
0.4
0.2
0.0
0
100
200
300
400
[SO2(g)]TOT mM
t= 25°C

Figure s2